

Iongel Soft Solid Electrolytes Based on [DEME][TFSI] Ionic Liquid for Low Polarization Lithium-O₂ Batteries

Marta Alvarez-Tirado,^[a, b] Laurent Castro,^{*[b]} Aurélie Guéguen,^[b] and David Mecerreyes^{*[a, c]}

Lithium-air/O₂ batteries are a promising battery technology for automotive applications due to their high energy density. However, many challenges need to be solved, particularly the high reactivity of the electrolyte with oxygen superoxide radicals and its low cyclability. In this work, we present a simple and fast way to prepare polymer-based iongel soft solid electrolytes. Thermally and mechanically stable iongels are

prepared by fast UV-photopolymerisation exhibiting a high ionic conductivity ($\sim 1.2 \times 10^{-3} \text{ S cm}^{-1}$ at 25 °C). When used as solid electrolytes in lithium symmetrical cells, they can withstand a critical current density of 0.5 mA cm⁻². Performance in Li–O₂ cells showed capacities as large as 3.3 mAh cm⁻², and cycling capability of 25 cycles, exceeding results on liquid-counterpart cells.

Introduction

Lithium-O₂ (Li–O₂) cells are a fascinating class of Li metal-air batteries featuring one of the highest theoretical specific energy densities (3500 Wh kg⁻¹).^[1] Nonetheless, there is still a long journey to go until their commercialization becomes a reality. From a material perspective, many efforts have been put in developing more efficient electrolytes that comply with a broad set of properties such as high ionic conductivity or more environmentally friendly electrolytes.^[2] In that sense, ionic liquids (ILs) seem a good alternative to conventional flammable organic solvents due to a combination of good transport properties, non-volatility, low toxicity (note that this property needs to be analyzed carefully),^[3] non-flammability and stability to superoxide radicals.^[4,5] The most investigated ionic liquids in Li–O₂ batteries are based on imidazolium- and pyrrolidinium-cations^[4,6–9] and fluorine-based anions (i.e., bis(trifluoromethanesulfonyl)imide, TFSI).^[10] Recently, less commonly used tetra-alkyl ammonium based ILs, such as N,N-diethyl-N-methyl-N-(2-methoxyethyl)ammonium bis(trifluoromethanesulfonyl)imide ([DEME][TFSI]) has shown suitable properties for application in this type of batteries. For

instance, Ulissi and co-workers^[11,12] showed that [DEME][TFSI] allowed a reversible, low polarization galvanostatic cycling in Li–O₂ cells. In other works,^[13] [DEME][TFSI] was used as electrolyte achieving 99.5% coulombic efficiency during cycling. Furthermore, the IL was able to create a lithium protective film when it was in contact with a Li_{1.5}Al_{0.5}Ge_{1.5}(PO₄)₃ (LAGP) solid inorganic film; improving in this way battery cyclability. On the other hand, liquid electrolyte batteries require a porous separator and leaking of the electrolyte is still a reality. A plausible way to further improve this is via the development of gel polymer electrolytes, in which the liquid electrolyte is safely encapsulated within a polymer network acting as a physical separator. They are also known as iongels, ionic liquid gels or ionogels if an IL-based electrolyte is used.^[14] Although this approach is quite popular in Li-ion,^[15–17] Li-metal,^[18–20] sodium-metal^[21,22] or other type of batteries,^[8,23] it has not been largely explored for Li–O₂ cells. There are a few examples based on poly(methyl) methacrylate (PMMA)^[24,25] or poly(vinylidene fluoride-co-hexafluoropropylene) (PVdF-HFP)^[26,27] polymer-based iongels. For instance, Zhao and co-workers^[25] developed by UV an iongel containing 1-ethyl-3-methylimidazolium tetrafluoroborate IL (EMIm-BF₄), dimethyl sulfoxide (DMSO) and LiTFSI, encapsulated in a polymer matrix formed by PMMA and a triacrylate. Lithium symmetrical cells containing this iongel presented overpotentials <0.1 V for 130 h when cycled at 0.3 mA h⁻¹. Lately, [DEME][TFSI] was selected to form a quasi-solid-state electrolyte by the gelation of this IL when mixed with multi-wall carbon nanotubes or solidification when mixed with Li_{6.40}La₃Zr_{1.40}Ta_{0.60}O₁₂ (LLZTO) ceramic nanoparticles via non-covalent interactions.^[28] Regarding salt concentration in ionic liquid based electrolytes, recent studies have shown that superconcentrated IL electrolytes (>1:1 molar ratio, IL:salt) are able to provide an efficient protection to lithium-metal^[29–32] or sodium-metal anodes.^[33] Interestingly, effect of salt concentration is deeply studied in IL-based liquid electrolytes for Li–O₂ applications^[34–36] but it is not largely evaluated when these are used in solid electrolytes. To the best of our knowledge, only one example could be found for iongels at high salt concentrations or all-solid-state sodium cells.^[21] In this research,

[a] M. Alvarez-Tirado, Prof. D. Mecerreyres
Innovative polymers
POLYMAT University of the Basque Country UPV/EHU
Avenida de Tolosa 72, Donostia-San Sebastian 20018, Spain
E-mail: david.mecerreyres@ehu.es

[b] M. Alvarez-Tirado, Dr. L. Castro, Dr. A. Guéguen
Material Engineering, Batteries
Toyota Motor Europe Research & Development 2
Hoge Wei 33 B, B-1930 Zaventem, Belgium
E-mail: Laurent.Castro@toyota-europe.com

[c] Prof. D. Mecerreyres
Ikerbasque
Basque Foundation for Science
E-48011 Bilbao, Spain

 Supporting information for this article is available on the WWW under <https://doi.org/10.1002/batt.202200049>

 © 2022 The Authors. *Batteries & Supercaps* published by Wiley-VCH GmbH. This is an open access article under the terms of the Creative Commons Attribution License, which permits use, distribution and reproduction in any medium, provided the original work is properly cited.

an iongel containing 50 mol% of NaFSI in a pyrrolidinium-based IL (N-propyl-N-methylpyrrolidinium bis(fluorosulfonyl)imide, C3mpyrFSI) is used as electrolyte. When used in sodium symmetrical cells, this highly-concentrated iongel was able to support higher current density cycling than an iongel containing 20 mol% of NaFSI.

In this work, we present a full study to obtain optimized solid polymer electrolytes for Li–O₂ batteries based on a low polarization ionic liquid ([DEME][TFSI]). Effects of salt concentration on a polymer-based electrolyte will be studied for the first time for Li–O₂ applications. By combining promising results of recent works, we present a simple but effective way of preparing iongels suitable for Li–O₂ cells that show mechanical and thermal stability, high ionic conductivity and battery performance, demonstrating equal or superior properties to the liquid-counterpart ionic liquid battery cells.

Results and Discussion

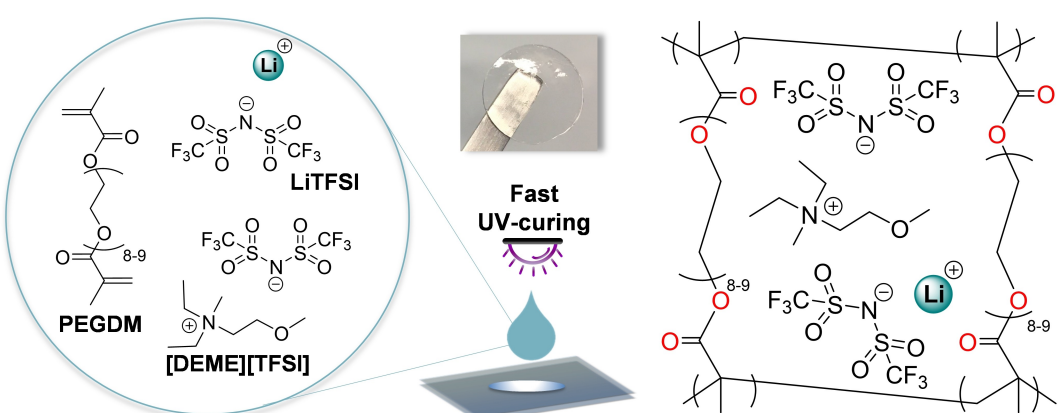
Iongels containing a liquid electrolyte based on [DEME][TFSI] ionic liquid and LiTFSI salt (ILE) were prepared by UV-photopolymerisation as previously shown for Li-ion and sodium-ion batteries.^[21,37,38] As shown in Scheme 1, poly(ethylene glycol) dimethacrylate (PEGDM) was directly mixed with the liquid electrolyte at different weight ratios (from 50 to 90 wt%, Table S1) in the presence of 2-hydroxy-2-methylpropiophene as the photoinitiator. After UV-irradiating for less than 2 min on the drop-casted solution, self-standing and transparent membranes were obtained. Samples with concentrations of ILE higher than 90 wt% were too soft (not self-standing) and difficult to handle. In all cases, the degree of cross-linking was monitored via Fourier transform infrared spectroscopy (FTIR) spectra, and conversions of $\geq 95\%$ were reached (Figure S1). The C=C stretching vibration of the acrylic groups (1640–1635 cm⁻¹) of the PEGDM dimethacrylate monomer significantly decreased/disappeared after the UV-irradiation, confirming high monomer conversion.^[39]

First, the impact of LiTFSI salt concentration on the physico-thermal properties of the iongels was assessed. Up to four

different molar concentrations of salt within the iongel were studied, including 13 mol%, 20 mol%, 32 mol% and 52 mol% of LiTFSI in [DEME][TFSI]. It is worth noting that only ILE in which the molar ratio of the salt is 52 mol%, is a super-concentrated one. Thus, an iongel with a 20 mol% of LiTFSI and 80% of ILE will be named as iongel-20 mol%-80. All combinations are described in Table S1.

The thermal stability of these iongels was evaluated through thermal gravimetric analysis, TGA. Iongels containing up to 90 wt% of ionic liquid electrolyte ILE were studied. As shown in Figure 1(a), all membranes did not present any thermal degradation until 315 °C due to the remarkable high thermal stability of [DEME][TFSI] ionic liquid (~325 °C decomposition temperature).^[40] Furthermore, the presence of higher LiTFSI concentrations did not significantly impact the results. On the other hand, their mechanical strength was evaluated through dynamic mechanical thermal analysis (DMTA), Figure 1(b). Results showed that the modulus and the membranes are stable from room temperature to high temperature (100 °C) due to its crosslinked nature whatever the ILE content. Larger content of polymer in the formulation provoked an increase of the membrane modulus (e.g., from 2×10^5 Pa to 4×10^5 Pa for iongel-20 mol%-90 and iongel-20 mol%-80, respectively). According to the Tan δ derivative, T_g decreased from -22.6 to -43.2 °C for iongel-TFSI-80 and iongel-TFSI-90, respectively. Hence, iongels with higher ILE content showed a lower glass transition value. Overall, the low T_g of these iongels and their mechanical robustness, even at very high ILE contents, together with their very high thermal stability, make these polymer electrolytes interesting materials for battery testing.

To down-select the most promising iongel compositions, their ionic conductivity (σ) at different temperatures was evaluated. As a baseline, [DEME][TFSI] based iongels with different ILE weight ratios but at fixed salt concentrations were assessed. Then, the most promising formulation (fixed ILE: polymer weight ratio) was used to evaluate the impact of salt concentration. Accordingly, iongels at increasing ILE weight ratios (50 wt%, 75 wt%, 80 wt%, 85 wt% and 90 wt%) were prepared at a fixed molar concentration of 13 mol% of LiTFSI in [DEME][TFSI] (Table S1). As shown in Figure 2(a), increasing



Scheme 1. Schematic representation of the rapid UV-photopolymerisation process undertaken to obtain the cross-linked iongel electrolytes.

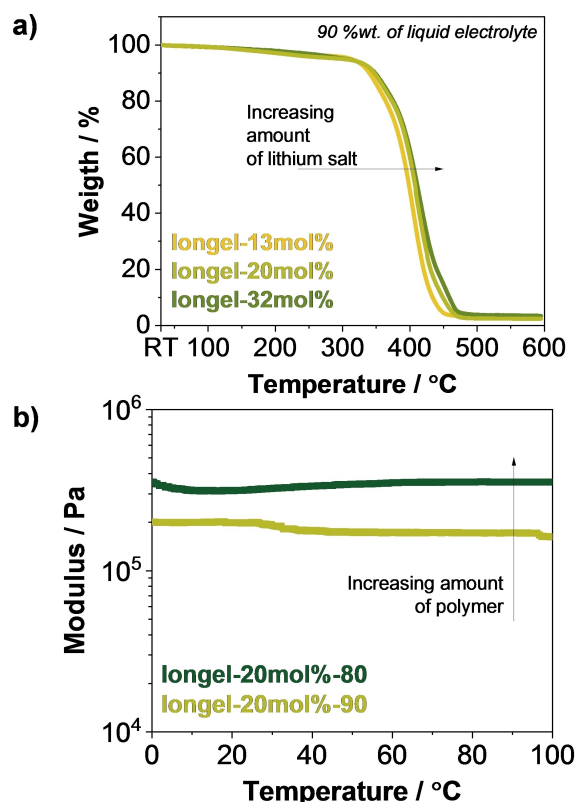


Figure 1. a) TGA analysis under nitrogen atmosphere at $10\text{ }^{\circ}\text{C min}^{-1}$ of iongel membranes containing 90 wt% liquid electrolyte; and b) DMTA analysis at compression from 0 to 100 $^{\circ}\text{C}$ of longel-20 mol% membranes containing 80 and 90 wt% of liquid electrolyte with same salt concentration (20 mol%).

weight ratios of the ILE leads to higher σ values. There was a difference of one order of magnitude between longel-13 mol%-50 and longel-13 mol%-90, achieving for the last composition a conductivity as high as $1.19 \times 10^{-3} \text{ S cm}^{-1}$ at 25 $^{\circ}\text{C}$, very close to the value of the liquid-counterpart at the same temperature ($1.96 \times 10^{-3} \text{ S cm}^{-1}$). The same trend was

found in iongels at 20 mol% LiTFSI molar concentration containing 80 wt%, 85 wt% and 90 wt% of LE (Figure S2), where longel-20 mol%-90 had the highest σ ($9.99 \times 10^{-4} \text{ S cm}^{-1}$ at 25 $^{\circ}\text{C}$). Hence, iongels containing 90 wt% of ILE was the chosen composition for further characterization.

Then, iongels with different LiTFSI concentrations were prepared (Figure 2b). As only iongels containing 90 wt% of ILE are studied from this point, only the molar ratio will be indicated in the nomenclature of the samples for simplicity (i.e., longel-52 mol%). As shown in Figure 2(b), iongels with lower salt concentrations lead to ionic conductivities two orders of magnitude higher than superconcentrated longel-52 mol% ($\sim 1.19 \times 10^{-3} \text{ S cm}^{-1}$ versus $6.35 \times 10^{-5} \text{ S cm}^{-1}$ at 25 $^{\circ}\text{C}$ for longel-13 mol% and longel-52 mol%, respectively). Relevant values at 25 $^{\circ}\text{C}$ and 60 $^{\circ}\text{C}$ are shown in Table S2.

In opposition to intuitive results, in which a higher concentration of ions would drive to higher ionic conductivities, the much higher viscosity of the superconcentrated ILE played a dominant role, leading to a higher resistance and slower ion transport.^[4,41] Similar conclusions were found in literature, where the increase in the [DEME][TFSI]-LiTFSI liquid electrolyte conductivity was directly related to a decrease in viscosity as per the Vogel-Fulcher-Tamman (VFT) model.^[11] Overall, iongels with 90 wt% of ILE and intermediate salt concentrations (13 or 20 mol%) showed the highest ionic conductivities, directly comparable to their liquid counterparts. Additionally, the pseudo-activation energy values for the ionic conduction process of these iongels were calculated following the Arrhenius-model for thermally activated processes^[42] (Figure S3). The calculated pseudo-energy values increased with higher salt concentration, and they were 0.31, 0.31, 0.33 and 0.48 eV for longel-13 mol%, longel-20 mol%, longel-32 mol% and longel-52 mol%, respectively (Figure S4). Hence, more diluted electrolytes (e.g., longel-13 mol% or longel-20 mol%) favored the decrease of E_a , facilitating ion transport. Furthermore, the fraction of current carried exclusively by the Li^+ ions, was also evaluated through the calculation of the lithium

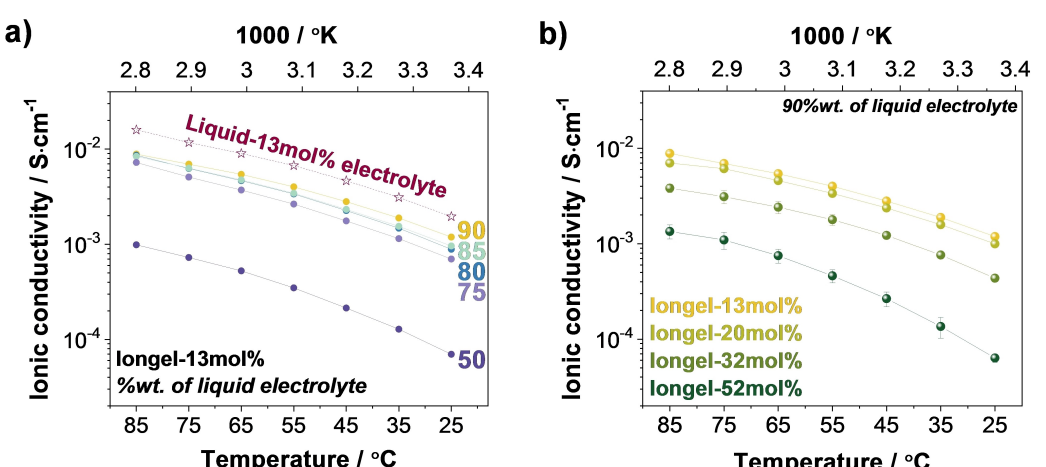


Figure 2. a) Ionic conductivity versus temperature of Liquid-13 mol% electrolyte and longel-13 mol% membranes containing increasing amounts of liquid electrolyte, from 50 to 90 wt%; and b) ionic conductivity versus temperature of iongel membranes containing 90 wt% of liquid electrolyte at increasing LiTFSI molar concentrations, from 13 mol% to 52 mol%. Inset: image of Ionogel-20 mol% membrane at 90 wt% liquid electrolyte.

transference number (t_{Li^+}) on lithium symmetrical cells at 60 °C. This was done following the well-known Evans-Vincent-Bruce method,^[43] where the cell is polarized by a small DC during a chronoamperometry (Figure S5). The results showed t_{Li^+} ranging between 0.10 and 0.14 (Figure 3a), increasing with increasing LiTFSI molar concentration. This same tendency was reported in other studies,^[31,44] in which the t_{Li^+} improved from 0.1 to 0.2 using highly-concentrated electrolytes suggesting different lithium-ion transport mechanisms for high concentrated systems.^[31] In lower concentrated ILE the ion pairs formed ($\text{Li} - [\text{TFSI}^-]_2$), do not favour Li transport and lowers t_{Li^+} ; however, in higher concentrated electrolytes, t_{Li^+} would be favoured via the Li–O atoms coordination formed between these TFSI-based aggregates.^[34]

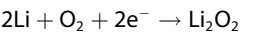
To determine the stability of these iongels against lithium metal, stripping/plating cycles at increasing current densities were performed on lithium symmetrical cells at 60 °C after 3 h conditioning at OCV.

This testing temperature was selected following the optimization work done by other research group with liquid cells using an ILE based on [DEME][TFSI].^[11] Current densities were increased from 0.01 to 1 mA cm⁻², cycled 3 times at each current with 1 h dwell. The average potential (in absolute value) achieved at each rate for each iongel cell is plotted in Figure 3(b). Cells with lower salt-concentrated iongel (i.e., longel-13 mol%, longel-20 mol% and longel-32 mol% cells) led to lower overpotentials, withstanding a critical current density

(CCD, chosen when potential exceeds 1 V) of 0.5 mA cm⁻². Unexpectedly, the superconcentrated longel-52 mol% cell had the lowest CCD (0.2 mA cm⁻²). Highly-concentrated ILE are usually explored to improve the stability against lithium metal, mitigating dendrites growth and improving stability of the solid electrolyte interface layer (SEI).^[31,44] The limited performance of the superconcentrated longel-52 mol% cell compared to literature could be related to the use of polymeric structures in this study, which might impact the SEI interfacial structure formed in pure superconcentrated liquid electrolyte cells,^[33,45] baseline of the good performance of these systems. Cells were further cycled (1 h plating, 1 h stripping) in galvanostatic mode at their CCD (Figure S6a). longel-13 mol% and longel-20 mol% cells behaved very similarly, with ~0.7 V overpotentials after 27 and 18 h, respectively. Then, they suffered from a “soft” short-circuit, showed off by voltage drops caused by lithium dendrites growth.^[46–48] Higher concentrated longel-32 mol% cells had lower overpotential (~0.2 V) for 14 h, and then showed a sharp polarization increase until cell death. Same test was also done on liquid equivalent cells (Figure S6b). They had a constant overpotential of ~0.2 V over cycling. Liquid-20 mol% cell was stable for 22 h, Liquid-32 mol% cell for 45 h and Liquid-13 mol% cells, the best out of the liquid cells, for 154 h; being in accordance with similar reported results.^[11]

Before testing in Li–O₂ cells, the stability window for upper potentials of the iongels were investigated in Li⁰/iongels/Stainless steel cells by cyclic voltammetry at a scan rate of 0.2 mV s⁻¹ at 60 °C (Figure S7). No significant differences were observed between longel-13 mol%, longel-20 mol% and longel-32 mol% cells, in which no oxidation currents occurred up to 3.72–3.78 V. The cell containing superconcentrated ILE(longel-52 mol%) showed a higher anodic stability, up to 3.98 V, in agreement to other studies on superconcentrated DEME-TFSI liquid cells.^[29,31] Following these results, cut-off potentials of 2 and 3.6 V were established for Li–O₂ cycling.

Swagelok Li–O₂ batteries were assembled and discharged in a dynamic mode at 60 °C to determine the maximum current rate at which the cells can operate (Figure 4a and b). Increasing current densities (from 5 μA cm⁻² to 0.28 mA cm⁻²) were applied for 15 min per rate. Steady potentials achieved at each rate are plotted in Figure 4a for all iongel cells (average of 3 cells per type). When the cells are discharged, the potential reaches a plateau at 2.96 V vs. Li⁰/Li⁺ (E_{eq}), which is the redox potential of the reaction:^[49]



This potential is usually ~0.3 V below and 0.5 V above the E_{eq} (at discharge and charge, respectively) due to energy loses. Results showed that cells containing intermediate salt concentrations ILE could be cycled at higher current rates (100 μA cm⁻² for longel-20 mol% and longel-32 mol% cells) than longel-13 mol% and longel-52 mol% cells (~75 μA cm⁻²). Considering all cells, 50 μA cm⁻² was selected as the maximum current density for further galvanostatic testing with an average discharge potential of ~2.6 V. Within liquid cells (Figure 4b),

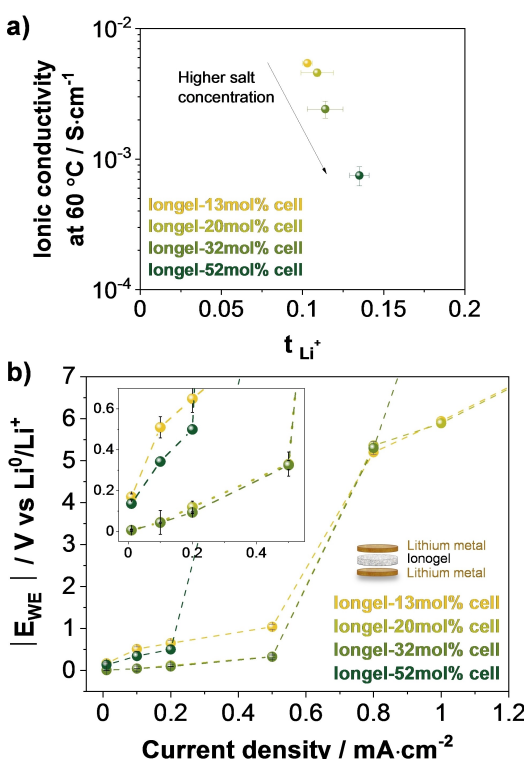


Figure 3. Tests on lithium symmetrical cells: a) Ionic conductivities at 60 °C against lithium transference number; and b) average potentials achieved at increasing current densities. Current densities were increased from 0.01 to 1 mA cm⁻² at 60 °C, cycled 3 times at each current with 1 h dwell.

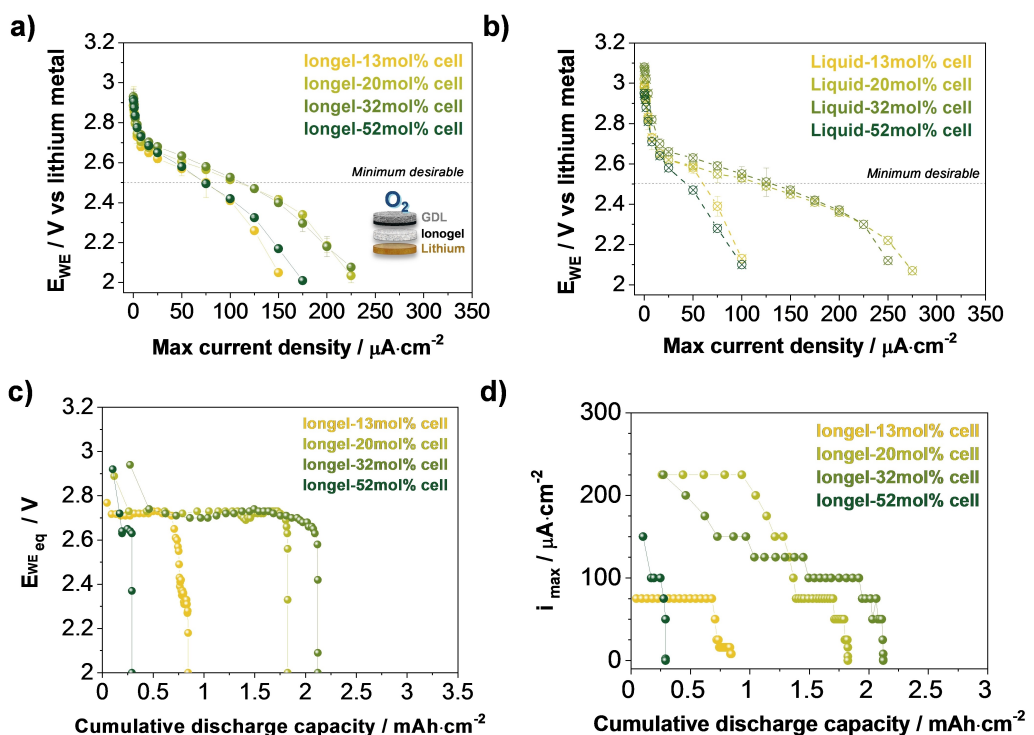


Figure 4. Dynamic discharge of Li–O₂ cells at 60 °C (rate test): discharge potential against current density at increasing LE salt concentrations of a) iongel cells and b) liquid cells; c) equilibrium polarization potential at OCV ($E_{1,\text{eq}}$, $E_{2,\text{eq}}$, etc.) against cumulative discharge capacity of longel cells achieved after each consecutive loops; and d) maximum current densities ($i_{\max 1}$, $i_{\max 2}$, etc.) achieved at the end of each discharge loop for the longel cells.

intermediate salt concentrations cells had the highest values (125 $\mu\text{A}\cdot\text{cm}^{-2}$ for Liquid-20 mol% and Liquid-32 mol% cells), similarly to iongel-based cells. This test was also carried out at 25 °C on cells with the lowest salt concentrations (13 mol% and 20 mol%, both liquid and polymeric cells) (Figure S8b). In these conditions, 20 $\mu\text{A}\cdot\text{cm}^{-2}$ seemed to be the maximum acceptable rate. Those rates were similar to the ones reported in literature for [DEME][TFSI] liquid cells at room temperature.^[11]

As seen in previous works,^[37] when a dynamic discharge loop is completed (Loop x1, Figure S9a), only a small portion of the cell discharge capacity is used (Figure S9b). Subsequently, as soon as the cell is no longer polarized (OCV), the potential tends to reach equilibrium over time, with $dE_{WE}/dt \sim 0$ ($E_{1,\text{eq}}$, $E_{2,\text{eq}}$, etc.). Once the potential is stable (usually closed to initial cell potential at OCV), cells can be discharged again. This operation (dynamic discharge) was repeated several times (i.e., Loop $\times 2$, Loop $\times 3$, ..., Loop $\times 150$), until no capacity was left and $E_{\text{eq}} \leq 2$ V. In every loop, cells were able to discharge until a specific current density, named as $i_{\max 1}$, $i_{\max 2}$, etc. These two sets of data – e.g., $E_{1,\text{eq}}$ and $i_{\max 1}$ – were used to analyze further the cells (Figures 4c, d and S9c, d). When the equilibrium polarization potentials at OCV ($E_{1,\text{eq}}$, $E_{2,\text{eq}}$, etc.) were plotted against the cumulative discharge capacities of the cell, the shape of the curve mimic the one of a galvanostatic discharge (Figure 4c). According to the results, cells with higher salt concentrations ILE led to higher cumulative capacities (32 mol% cells > 20 mol% cells > 13 mol% cells). This could be explained as the equilibrium potentials are proportional to the amount of mobile ions present in the electrolyte (higher polarization effect

for higher ion-concentrated ILE). This rule was no longer applied on the superconcentrated ILE (52 mol%), in which the viscosity kept being the dominant resistance force for ion transport and ion mobility was then significantly reduced (low polarization). Furthermore (Figure S9c), iongel-based cells presented lower polarizations than liquid cells (lower cumulative capacities) and 0.1 V difference in equilibrium potentials (2.7 and 2.8 V for iongel and liquid cells, respectively). On the other hand, the maximum currents achieved on each loop ($i_{\max 1}$, $i_{\max 2}$, etc.) played an important role too in the final cumulative discharge capacity. Figures 4(d) and S6(d) show how these current rates were much higher during the full cell discharge for longel-20 mol% and longel-32 mol% cells, with maximums of 225 $\mu\text{A}\cdot\text{cm}^{-2}$ (~125 $\mu\text{A}\cdot\text{cm}^{-2}$ for the rest of the cells), and matching previous results.

Afterwards, Li–O₂ iongel cells were fully discharged/charged in galvanostatic mode at the selected rate (50 $\mu\text{A}\cdot\text{cm}^{-2}$), temperature (60 °C), using 100 μL of catholyte (Figure S8a) and after 3 h conditioning at OCV. Figure 5(a) shows that the absolute discharge capacity of longel-13 mol% cell (3.3 $\text{mAh}\cdot\text{cm}^{-2}$) was the highest of the group and three times higher than superconcentrated longel-52 mol% cell. However, longel-20 mol% cell has the highest Coulombic efficiency (100%, 2.5 $\text{mAh}\cdot\text{cm}^{-2}$). This fully discharged/charged test was also done at a higher rate (0.1 $\text{mA}\cdot\text{cm}^{-2}$), obtaining lower capacities (~0.7 $\text{mAh}\cdot\text{cm}^{-2}$, iongel cells) and confirming the optimization results obtained on the dynamic discharge test (Figure S10a, b). Due to their lack of performance, superconcentrated cells were not tested further. Lastly, Li–O₂ cells

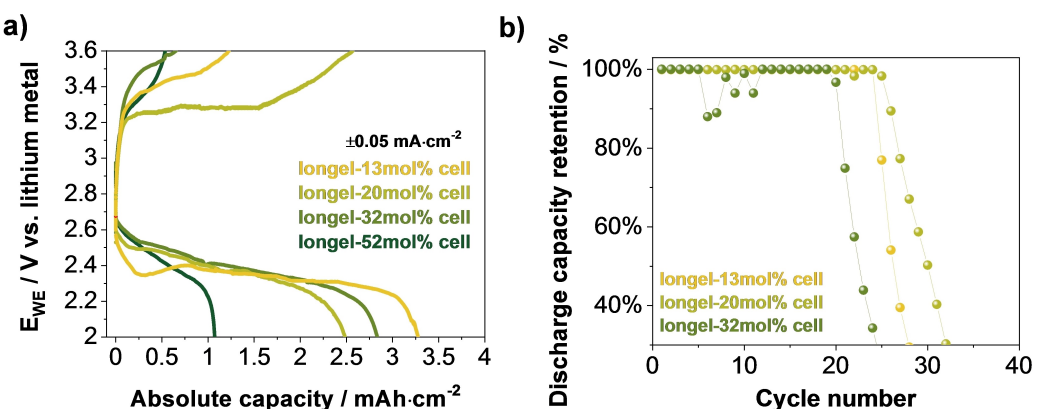


Figure 5. Galvanostatic discharge/charge of Swagelok Li–O₂ cells at 60°C: a) Potential against absolute capacity plot at $\pm 0.05 \text{ mA cm}^{-2}$, and b) discharge capacity retention during cycling of iongel cells, cycled at $\pm 0.05 \text{ mA cm}^{-2}$ with limited capacity (0.2 mAh cm^{-2}).

were cycled with limited capacity (0.2 mA cm^{-2}) at $50 \mu\text{A cm}^{-2}$ and 2–3.6 V cut-off potentials. Figure 5(b) displays the discharge capacity retention of the three iongel cells. The best ones, longel-13 mol % and longel-20 mol % cells started to fade after 25 cycles, although the fading of the 20 mol % one is slightly smoother. In terms of Coulombic efficiency, CE, (Figure S10d), the longel-20 mol % cell had a 100% CE for a few cycles more than longel-13 mol % cell. The cyclability of the liquid cells was also undertaken for comparison (Figure S10c). Liquid-13 mol % cell was the best one, keeping 100% of the discharge capacity for 22 cycles. Thus, based on all these electrochemical tests, we can conclude that in our case iongel-based cells had higher cyclability than liquid cells.

Conclusion

In this work we present a step forward in the development of safer electrolyte designs for Li–O₂ batteries by the use of soft solid iongel electrolytes based on a low polarization ionic liquid electrolyte. Taking the best of previous research works, iongel polymeric electrolytes have been optimized by varying the polymer: ionic liquid electrolyte ratios, and the salt concentration, including superconcentrated electrolytes. The iongels can be prepared in an easy but effective manner (fast UV-polymerization) as flexible and self-standing membranes. The ionic nature of the liquid electrolyte made these iongels exceptionally thermally stable (no degradation until 315°C), and sufficiently robust ($\sim 10^5 \text{ Pa}$) for battery cells operations. Even further, the optimization of the formulation allowed finding iongels with an ionic conductivity close to the liquid counterpart ($\sim 1.2 \times 10^{-3} \text{ S cm}^{-1}$ at 25°C). Intermediate salt-concentrated iongels (20 mol%), showed excellent performance in lithium symmetrical cells, exceeding the liquid cells results. Overall, longel-20 mol % Li–O₂ cells exhibited a compromising performance amongst the rest of the cells: one of the maximum current rates, higher number of cycles and highest Coulombic efficiency. The findings would also confirm the capability and performance of the polymeric-based electrolytes in this type of batteries, which is directly comparable to

liquid cells. This optimized and fast preparation method of ionic liquid solid electrolytes could be used as the baseline for future works in which iongel properties could be tuned for application in Li–O₂ technology.

Experimental Section

Comprehensive experimental details including synthesis and characterizations can be found in the Supporting Information.

Acknowledgements

This work was supported by the European Commission's funded Marie Skłodowska-Curie project POLYTE-EID (Project No. 765828). The manuscript was written through contributions of all authors that have given approval to the final version.

Conflict of Interest

The authors declare no conflict of interest.

Data Availability Statement

The data that support the findings of this study are available from the corresponding author upon reasonable request.

Keywords: iongel · lithium-O₂ battery · lithium metal · polymer electrolyte · solid-state battery

- [1] W.-J. Kwak, Rosy, D. Sharon, C. Xia, H. Kim, L. R. Johnson, P. G. Bruce, L. F. Nazar, Y.-K. Sun, A. A. Frimer, M. Noked, S. A. Freunberger, D. Aurbach, *Chem. Rev.* **2020**, *120*, 6626–6683.
- [2] D. Wang, X. Mu, P. He, H. Zhou, *Mater. Today* **2019**, *26*, 87–99.
- [3] J. Flieger, M. Flieger, *Int. J. Mol. Sci.* **2020**, *21*, 1–41.
- [4] K. Liu, Z. Wang, L. Shi, S. Jungsuttiwong, S. Yuan, *J. Energy Chem.* **2020**, *59*, 320–333.

- [5] T. Stettner, A. Balducci, *Energy Storage Mater.* **2021**, *40*, 402–414.
- [6] L. Long, S. Wang, M. Xiao, Y. Meng, *J. Mater. Chem. A* **2016**, *4*, 10038–10039.
- [7] E. Knipping, C. Aucher, G. Guirado, L. Aubouy, *New J. Chem.* **2018**, *42*, 4693–4699.
- [8] Q. Yang, Z. Zhang, X. G. Sun, Y. S. Hu, H. Xing, S. Dai, *Chem. Soc. Rev.* **2018**, *47*, 2020–2064.
- [9] H. Nakamoto, Y. Suzuki, T. Shiotsuki, F. Mizuno, S. Higashi, K. Takechi, T. Asaoka, H. Nishikoori, H. Iba, *J. Power Sources* **2013**, *243*, 19–23.
- [10] T. Rüther, A. I. Bhatt, A. S. Best, K. R. Harris, A. F. Hollenkamp, *Batteries & Supercaps* **2020**, *3*, 793–827.
- [11] U. Ulissi, G. A. Elia, S. Jeong, F. Mueller, J. Reiter, N. Tsiovaras, Y. K. Sun, B. Scrosati, S. Passerini, J. Hassoun, *ChemSusChem* **2018**, *11*, 229–236.
- [12] U. Ulissi, G. A. Elia, S. Jeong, J. Reiter, N. Tsiovaras, S. Passerini, J. Hassoun, *Chem. A Eur. J.* **2018**, *24*, 3178–3185.
- [13] X. P. Zhang, Z. Y. Wen, T. Zhang, *J. Mater. Chem. A* **2018**, *6*, 12945–12949.
- [14] M. Forsyth, L. Porcarelli, X. Wang, N. Goujon, D. Mecerreyes, *Acc. Chem. Res.* **2019**, *52*, 686–694.
- [15] L. Liang, X. Chen, W. Yuan, H. Chen, H. Liao, Y. Zhang, *ACS Appl. Mater. Interfaces* **2021**, DOI 10.1021/acsami.1c06077.
- [16] Z. Ma, J. Liu, J. Fei, N. He, P. Wang, J. Wang, Z. Chen, Z. Ji, H. Wang, W. Ling, N. Nie, M. Hu, Y. Huang, *ChemElectroChem* **2020**, *7*, 3998–4002.
- [17] W. J. Hyun, C. M. Thomas, N. S. Luu, M. C. Hersam, *Adv. Mater.* **2021**, *33*, 1–8.
- [18] Z. Chen, Y. Yang, Q. Su, S. Huang, D. Song, R. Ma, C. Zhu, G. Lv, C. Li, *ACS Appl. Mater. Interfaces* **2021**, DOI 10.1021/acsami.1c07745.
- [19] J. Tang, B. Zhai, J. Liu, W. Ren, Y. Han, H. Yang, Y. Chen, C. Zhao, Y. Fang, *Phys. Chem. Chem. Phys.* **2021**, *23*, 6775–6782.
- [20] A. Su, P. Guo, J. Li, D. Kan, Q. Pang, T. Li, J. Sun, G. Chen, Y. Wei, *J. Mater. Chem. A* **2020**, *8*, 4775–4783.
- [21] A. F. De Anastro, L. Porcarelli, M. Hilder, C. Berlanga, M. Galceran, P. Howlett, M. Forsyth, D. Mecerreyes, *ACS Appl. Energ. Mater.* **2019**, *2*, 6960–6966.
- [22] T. A. Ha, A. Fdz De Anastro, N. Ortiz-Vitoriano, J. Fang, D. R. MacFarlane, M. Forsyth, D. Mecerreyes, P. C. Howlett, C. Pozo-Gonzalo, *J. Phys. Chem. Lett.* **2019**, *10*, 7050–7055.
- [23] W. J. Hyun, C. M. Thomas, M. C. Hersam, *Adv. Energy Mater.* **2020**, *10*, 1–7.
- [24] C. V. Amanchukwu, H.-H. Chang, M. Gauthier, S. Feng, T. P. Batcho, P. T. Hammond, *Chem. Mater.* **2016**, *28*, 7167–7177.
- [25] H. Zhao, X. Liu, Z. Chi, S. Chen, S. Li, Z. Guo, L. Wang, *Appl. Surf. Sci.* **2021**, *565*, 150612.
- [26] J. Pan, H. Li, H. Sun, Y. Zhang, L. Wang, M. Liao, X. Sun, H. Peng, *Small* **2018**, *14*, 1–6.
- [27] K. N. Jung, J. I. Lee, J. H. Jung, K. H. Shin, J. W. Lee, *Chem. Commun.* **2014**, *50*, 5458–5461.
- [28] K. N. Gao, H. R. Wang, M. H. He, Y. Q. Li, Z. H. Cui, Y. Mao, T. Zhang, *J. Power Sources* **2020**, *463*, 228179.
- [29] X. Gao, F. Wu, A. Mariani, S. Passerini, *ChemSusChem* **2019**, *12*, 4185–4193.
- [30] T. Shiga, Y. Masuoka, H. Nozaki, *RSC Adv.* **2021**, *11*, 13359–13365.
- [31] K. Periyapperuma, E. Arca, S. Harvey, C. Ban, A. Burrell, D. R. Macfarlane, C. Pozo-Gonzalo, M. Forsyth, P. C. Howlett, *J. Mater. Chem. A* **2020**, *8*, 3574–3579.
- [32] X. Wang, R. Kerr, F. Chen, N. Goujon, J. M. Pringle, D. Mecerreyes, M. Forsyth, P. C. Howlett, *Adv. Mater.* **2020**, *32*, DOI 10.1002/adma.201905219.
- [33] D. A. Rakov, F. Chen, S. A. Ferdousi, H. Li, T. Pathirana, A. N. Simonov, P. C. Howlett, R. Atkin, M. Forsyth, *Nat. Mater.* **2020**, *19*, 1096–1101.
- [34] Y. Cai, Q. Zhang, Y. Lu, Z. Hao, Y. Ni, J. Chen, *Angew. Chem. Int. Ed.* **2021**, *300071*, 25973–25980.
- [35] H. Zhang, W. Qu, N. Chen, Y. Huang, L. Li, F. Wu, R. Chen, *Electrochim. Acta* **2018**, *285*, 78–85.
- [36] C. Liu, X. Ma, F. Xu, L. Zheng, H. Zhang, W. Feng, X. Huang, M. Armand, J. Nie, H. Chen, Z. Zhou, *Electrochim. Acta* **2014**, *149*, 370–385.
- [37] M. Alvarez Tirado, L. Castro, G. Guzmán-González, L. Porcarelli, D. Mecerreyes, *ACS Appl. Energ. Mater.* **2021**, *4*, 295–302.
- [38] C. Gerbaldi, J. R. Nair, S. Ahmad, G. Meligrana, R. Bongiovanni, S. Bodoardo, N. Penazzi, *J. Power Sources* **2010**, *195*, 1706–1713.
- [39] V. Vijayakumar, B. Anothumakkool, S. Kurungot, M. Winter, J. R. Nair, *Energy Environ. Sci.* **2021**, *14*, 2708–2788.
- [40] G. Vanhoutte, S. D. Hojniak, F. Bardé, K. Binnemans, J. Fransaera, *RSC Adv.* **2018**, *8*, 4525–4530.
- [41] S. Drvarić Talian, M. Bešter-Rogač, R. Dominko, *Electrochim. Acta* **2017**, *252*, 147–153.
- [42] S. B. Aziz, T. J. Woo, M. F. Z. Kadir, H. M. Ahmed, *J. Sci. Adv. Mater. Devices* **2018**, *3*, 1–17.
- [43] S. Zugmann, M. Fleischmann, M. Amereller, R. M. Gschwind, H. D. Wiemhöfer, H. J. Gores, *Electrochim. Acta* **2011**, *56*, 3926–3933.
- [44] J. Tong, S. Wu, N. von Solms, X. Liang, F. Huo, Q. Zhou, H. He, S. Zhang, *Front. Chem.* **2020**, *7*, 1–10.
- [45] K. Periyapperuma, E. Arca, S. Harvey, T. Pathirana, C. Ban, A. Burrell, C. Pozo-Gonzalo, P. C. Howlett, *ACS Appl. Mater. Interfaces* **2020**, *12*, 42236–42247.
- [46] D. Kang, N. Hart, M. Xiao, J. P. Lemmon, *Wuli Huaxue Xuebao/Acta Phys. Chim. Sin.* **2021**, *37*, 1–6.
- [47] Z. Chen, G. T. Kim, J. K. Kim, M. Zarrabeitia, M. Kuenzel, H. P. Liang, D. Geiger, U. Kaiser, S. Passerini, *Adv. Energy Mater.* **2021**, *11*, DOI 10.1002/aenm.202101339.
- [48] B. Wu, J. Lochala, T. Taverne, J. Xiao, *Nano Energy* **2017**, *40*, 34–41.
- [49] Y. Wang, N. C. Lai, Y. R. Lu, Y. Zhou, C. L. Dong, Y. C. Lu, *Joule* **2018**, *2*, 2364–2380.

Manuscript received: January 28, 2022

Revised manuscript received: March 11, 2022

Accepted manuscript online: March 14, 2022

Version of record online: March 25, 2022